Local tunneling characteristics near a grain boundary of a *d*-wave superconductor as probed by a normal-metal or a low-T_c-superconductor STM tip

Hongwei Zhao and Chia-Ren Hu
Department of Physics, Texas A & M University, College Station, Texas 77843-4242
(Received 29 November 1999)

We study the local single-particle tunneling characteristics [as observed with scanning tunnel microscopy (STM)] for *N-D* and *S-D* tunneling, where *D* is a *d*-wave superconductor with a {100}|{110} grain boundary. The tunneling Hamiltonian method is used. The self-consistent order parameter is first determined using the quasiclassical Green's-function method, and then the tunneling characteristics at various distances from the interface, reflectivity of the interface, and temperature, are studied. For *N-D* tunneling, a zero-bias conductance peak (ZBCP) occurs near the interface, with diminishing magnitude away from it. For *S-D* tunneling, the ZBCP splits to exhibit the gap of the *s*-wave low-T_c superconducting tunneling tip, and there is a range of negative conductance just outside the peaks, when the tunneling point is near the grain boundary. The results are compared with those obtained by using a constant order parameter in each grain.

I. INTRODUCTION

There has been a large number of experiments studying the symmetry of the order parameter in high-T_c superconductors (HTSC's), because this information is crucial for understanding the mechanism of this class of superconductors. Several phase-sensitive experiments[1–3] have observed the sign change of the order parameter on the essentially cylindrical Fermi surface, which supports the conclusion that the order parameter of HTSC's has predominantly a $d_{x^2-y^2}$-wave symmetry.

For the $d_{x^2-y^2}$-symmetry model, the existence of zero-energy (quasiparticle) bound states (ZEBS's, also called the midgap states) on the surface has been predicted.[4] The reason for their existence is that the incident and reflected quasiparticles see different signs of the order parameter. The number of the ZEBS's depends on the orientation of the surface with respect to the crystal axis. It has a maximum for a {110} surface and a minimum (i.e., zero) for a {100} surface.[5] (According to Refs. 6 and 7, the ZEBS's can also exist on a microscopically rough {100} surface.) The discussion can be directly generalized to an interface (i.e., a grain boundary) of a *d*-wave superconductor, but the condition for the existence of the ZEBS's is more restrictive.[8,9] Namely, both the reflected and the transmitted quasiparticles have to see different signs of the order parameter from that seen by the incident quasiparticle. The ZEBS's can lead to a zero-bias conductance peak (ZBCP) in quasiparticle tunneling,[4,10] which has been observed in many experiments.[11–24] Fogelstrom, Rainer, and Sauls[6] then concluded that a pure *d*-wave order parameter can induce an *s*-wave subdominant component near the surface because of the strong pair breaking property of the latter. The two order-parameter components have a relative phase difference of $\pi/2$, and the resultant $d+is$ order parameter near the surface gives rise to a broken time-reversal symmetry (BTRS) state, which causes the energy of a ZEBS to shift away from zero by an amount which is dependent on its momentum along the surface in the *ab* plane. This energy shift gives rise to a splitting of the ZBCP at zero magnetic field and further nonlinear splitting with increasing external field, which appears to have been observed.[22]

Originally, the observed ZBCP was analyzed in terms of the spin-flip and Kondo scatterings from the magnetic impurities which were presumed to exist at or near the interface. But this interpretation has been challenged by the experimentally observed[17,20] *nonlinear* dependence of the ZBCP splitting on the applied magnetic field, and also by the absence of a ZBCP for the electron-doped, presumably *s*-wave cuprate superconductors.[17–19,25] Furthermore, that the ZBCP is continuously observed with STM for a long distance (160 nm) on a {110} surface, with nearly a constant height, is strongly against the impurities scenario;[16] and that a ZBCP is consistently observed on a {110} surface, and consistently not observed on a {100} surface, is also strongly in favor of the midgap-states scenario.[24] Therefore the observation of the ZBCP in HTSC's can nowadays be regarded as a strong evidence for the $d_{x^2-y^2}$-wave order-parameter symmetry in this class of SC's (which probably does not include the electron-doped cuprates). The ZBCP was also observed on the {100} surface[23] which is attributed to the roughness of the surface.[6,7] For tunneling between a low-T_c superconductor (LTSC) and a HTSC, a splitting of the ZBCP at zero magnetic field was observed,[11] and the conductance at zero bias decreases with decreasing temperature. Because this splitting only occurs when the temperature is below the T_c of the LTSC, it cannot be attributed to the BTRS states. It is explained as due to the convolution between the quasiparticle density of states of the LTSC and that of the HTSC.[8]

The ZEBS is a quasiparticle state localized near a surface or an interface. We expect that this localization can be observed in an STM-type of localized quasiparticle tunneling: The ZBCP is expected to have a maximum height when the tunneling occurs at the surface or interface and to decrease in height when the tunneling point moves away from the surface or interface.[26] In this paper, we study the local characteristics for tunneling between an STM tip and a *d*-wave superconductor with a grain boundary (as shown in Fig. 1).[27]

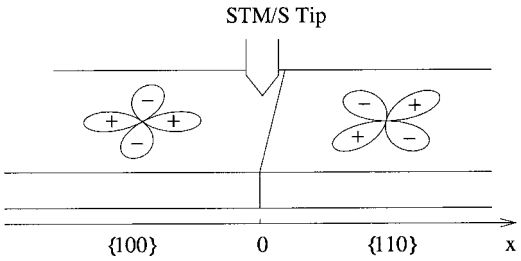

FIG. 1. Schematic drawing showing an STM tip scanning the vicinity of a {100}|{110} grain boundary of a *d*-wave superconductor. The tunneling direction is along the *c* axis in this figure, but it does not have to be so.

We assume that the left grain is {100} oriented and the right grain is {110} oriented. The angular dependence of the order parameter is $\Delta_L(\theta)=\cos(2\theta)$ and $\Delta_R(\theta)=\sin(2\theta)$, for the left and right grains, respectively, where θ is the angle between a two-dimensional momentum vector in the *ab* plane and the surface normal. When the tip scans in the *xy* plane, the tunneling can occur at different points relative to the grain boundary. A HTSC can, to a good approximation, be considered as a two-dimensional (2D) system. If we assume translational invariance along the grain boundary, we expect the spatial dependence of the tunneling characteristics to depend on one coordinate only, viz., the coordinate *x* measured perpendicular to the grain boundary. We will study the local tunneling characteristics when the tip is either a normal metal (*N*) or a LTSC (*S*).

This paper is organized as follows: Sec. II briefly introduces the method of quasiclassical Green's functions for the calculation of the self-consistent order parameter. In Secs. III and IV, we present the tunneling conductance for the tip being a normal metal and a LTSC, respectively. Finally, we make brief conclusions in Sec. V.

II. SELF-CONSISTENT ORDER PARAMETER

The situation we considered is shown in Fig. 1. The grain boundary (interface) is located at $x=0$. We assume that the left-hand side of the interface is a {100} grain and the right-hand side is a {110} grain. An STM-type tunneling can occur at different distances (i.e., *x*'s) away from the interface. In order to calculate the tunneling conductance accurately at different tunneling points, first we need to calculate the spatially varying self-consistent order parameter. We use the quasiclassical Green's-function method[28–30] to calculate this quantity. The order parameter can be expressed as

$$\Delta(\mathbf{r},\mathbf{r}')=V(\mathbf{r},\mathbf{r}')\langle\Psi_{\uparrow}(\mathbf{r})\Psi_{\downarrow}(\mathbf{r}')\rangle = TV(\mathbf{r},\mathbf{r}')\sum_n\sum_l \frac{u_l(\mathbf{r})v_l^*(\mathbf{r}')}{i\varepsilon_n-E_l}, \tag{1}$$

where $V(\mathbf{r},\mathbf{r}')$ is the pair interaction, T is the absolute temperature, ε_n is the Matsubara frequency, and $\varepsilon_n=(2n+1)\pi T$; u_l and v_l satisfy the Bogoliubov–de Gennes equations with eigenenergy E_l:

$$E_l u_l(\mathbf{x_1})=\hat{h}_0 u_l(\mathbf{x_1})+\int \Delta(\mathbf{s},\mathbf{r})v_l(\mathbf{x_2})d\mathbf{x_2}, \tag{2}$$

$$E_l v_l(\mathbf{x_1})=-\hat{h}_0 v_l(\mathbf{x_1})+\int \Delta(\mathbf{s},\mathbf{r})u_l(\mathbf{x_2})d\mathbf{x_2}, \tag{3}$$

where $\mathbf{s}\equiv(\mathbf{x_1}-\mathbf{x_2})$, $\mathbf{r}\equiv(\mathbf{x_1}+\mathbf{x_2})/2$, and $\hat{h}_0\equiv-\hbar^2\nabla^2_{\mathbf{x_1}}/2m-\mu$ in the absence of a magnetic field and any other fields, with μ the chemical potential. In the WKBJ approximation, the wave function has the form

$$\begin{pmatrix} u(\mathbf{x}) \\ v(\mathbf{x}) \end{pmatrix}=e^{i\mathbf{k_F}\cdot\mathbf{x}}\begin{pmatrix} \overline{u}(x) \\ \overline{v}(x) \end{pmatrix}, \tag{4}$$

where k_F is the Fermi momentum. $\overline{u}(x)$ and $\overline{v}(x)$ vary on a scale of the coherent length ξ_0, which is much larger than the Fermi wave length k_F^{-1}. According to the 2D property of HTSC's, and if we assume the translational invariance of the interface, $\overline{u}$, $\overline{v}$, and Δ depend on *x* only. Substitution of Eq. (4) into Eqs. (2) and (3) and neglecting the second-order differential terms lead to the Andreev equations

$$E\overline{u}(x)=-iv_{Fx}\frac{d}{dx}\overline{u}(x)+\Delta(\hat{\mathbf{k}},x)\overline{v}(x), \tag{5}$$

$$E\overline{v}(x)=iv_{Fx}\frac{d}{dx}\overline{v}(x)+\Delta(\hat{k},x)\overline{u}(x), \tag{6}$$

where $\Delta(\mathbf{k},x)$ is the order parameter after a Fourier transformation with respect to the relative coordinate **s**; i.e., **k** is the relative wave vector. v_{Fx} is the *x* component of the Fermi velocity along **k**. For the order parameter in Eqs. (5) and (6), only the direction of the wave vector, $\hat{\mathbf{k}}=\mathbf{k}/|\mathbf{k}|$, is retained as a variable, because the momentum can be fixed on the Fermi surface in the weak-coupling treatment. To simplify the notation, we have suppressed the $\hat{\mathbf{k}}$ dependence in $\overline{u}$ and $\overline{v}$.

If we assume partial specular reflection (with probability *r*) and partial forward transmission (with probability $t=1-r$) at the interface, the *y* component of the momentum of a quasiparticle will be still k_y after a reflection, but the *x* component of the momentum will change sign. Therefore the wave function should be a linear combination of two terms on each side of the interface:

$$\begin{pmatrix} u_l(x,y) \\ v_l(x,y) \end{pmatrix}=e^{ik_y y}\sum_{\alpha=+,-}\phi_{l\alpha}(x,\theta_\alpha)e^{\alpha ik_x x}, \tag{7}$$

where θ_α measures the direction of the momentum $(\alpha k_x, k_y)$ with respect to the *x* axis. + and − mean right and left moving, respectively. $\theta_+=\theta$ with $-\pi/2<\theta<\pi/2$ gives the direction of a right-moving electron, and $\theta_-=\pi-\theta$ gives that of a left-moving electron. $k_x=k_F\cos\theta>0$ and $k_y=k_F\sin\theta$ are the *x* and *y* components of a right-going momentum vector, respectively, and

$$\phi_{l\alpha}=\begin{pmatrix} \overline{u}_{l\alpha} \\ \overline{v}_{l\alpha} \end{pmatrix}. \tag{8}$$

After applying a Fourier transformation to Eq. (1), the order parameter can be expressed as[28,29,31]

$$\Delta(\theta,x)=\frac{Tm}{4\pi}\sum_{n,\alpha=\pm}\int_{-\pi/2}^{\pi/2}d\theta'[\hat{g}_{\alpha\alpha}(x,\theta'_\alpha,\varepsilon_n)V(\theta,\theta'_\alpha)]_{12}, \tag{9}$$

where each $\hat{g}_{\alpha\beta}$ is a 2×2 matrix in the particle-hole space. It is known as the quasiclassical Green's function. The subscript 12 means the element 12 of this matrix. The defining equation

$$\hat{g}_{\alpha\beta}(x)\pm i(\gamma_3)_{\alpha\beta}\hat{1}=-2\upsilon_{Fx}\hat{\rho}_3\hat{G}_{\alpha\beta}(x\pm0,x), \tag{10}$$

relates $\hat{g}_{\alpha\beta}$ to $\hat{G}_{\alpha\beta}(x,x')$, which is the Gor'kov Green's function, a 2×2 matrix in the particle-hole space, further converted to a 2×2 matrix in the ''directional space,'' with indices $\alpha\beta$, so that the rapidly oscillating factors can be removed:[28]

$$\hat{G}_{\alpha\beta}(x,x')=\sum_l \frac{\phi_{l\alpha}(x)\phi^+_{l\beta}(x')}{i\varepsilon_n-E_l}, \tag{11}$$

where the l sum is now confined to the sum over the quantum number in association with the x motion only, since the sum over k_y has been turned into an integral over θ' in Eq. (9). [The l sum in Eq. (1) includes the sum over both quantum numbers.] In Eq. (10), γ_3 is the third Pauli matrix in the directional (i.e., $+\ -$) space, ρ_3 is the third Pauli matrix in the particle-hole space, and $\hat{1}$ is the unit matrix in the particle-hole space. To simplify the notation, we have left out the variables θ and ε_n in $\hat{g}_{\alpha\beta}$ and $\hat{G}_{\alpha\beta}$ in Eqs. (10) and (11). In Eq. (9), We have omitted the $\hat{g}_{+-}$ and $\hat{g}_{-+}$ terms because their contributions are rapidly oscillating in the scale of Fermi wavelength. The quasiclassical Green's function $\hat{g}_{\alpha\beta}$ satisfies the following differential equation:[29]

$$i\upsilon_{F_x}\partial_x\hat{g}_{\alpha\beta}=-\alpha(i\varepsilon_n\hat{1}-\hat{\Delta}_\alpha)\hat{\rho}_3\hat{g}_{\alpha\beta}+\hat{g}_{\alpha\beta}\beta(i\varepsilon_n\hat{1}-\hat{\Delta}_\beta)\hat{\rho}_3, \tag{12}$$

where

$$\hat{\Delta}_\alpha=\begin{pmatrix}0 & \Delta(\theta_\alpha,x)\\ \Delta^*(\theta_\alpha,x) & 0\end{pmatrix}. \tag{13}$$

In order to solve the differential Eq. (12), we need the boundary conditions of the quasiclassical Green's function $\hat{g}_{\alpha\beta}$ at the interface and the two end points: $x=-L_L$ and L_R. (Eventually, we will let L_L and L_R go to infinity.) The boundary condition at the interface is[28]

$$\tilde{g}^L(0)=\tilde{M}\tilde{g}^R(0)\tilde{M}^+, \tag{14}$$

where $\tilde{g}$ is a 2×2 matrix in the directional (i.e., $+\ -$) space with elements $\hat{g}_{\alpha\beta}$, each of which is a 2×2 matrix in the particle-hole space. $\tilde{M}$ is also a 2×2 matrix in the directional space, of the form

$$\tilde{M}=\begin{pmatrix}\dfrac{1}{c_d} & \dfrac{c_r^*}{c_d^*}\\ \dfrac{c_r}{c_d} & \dfrac{1}{c_d^*}\end{pmatrix}, \tag{15}$$

where c_r and c_d are the reflection and transmission coefficients (i.e., probability amplitudes), respectively. The boundary conditions at the two ends $x=-L_L$ and $x=L_R$ are[28]

$$\begin{aligned}
\hat{g}^L_{++}(-L_L)+i&=\hat{g}^L_{--}(-L_L)+i=-e^{-i\eta_L}\hat{g}^L_{+-}(-L_L),\\
\hat{g}^L_{++}(-L_L)-i&=\hat{g}^L_{--}(-L_L)-i=-e^{i\eta_L}\hat{g}^L_{-+}(-L_L),\\
\hat{g}^R_{++}(L_R)+i&=\hat{g}^R_{--}(L_R)+i=-e^{-i\eta_R}\hat{g}^R_{-+}(L_R),\\
\hat{g}^R_{++}(L_R)-i&=\hat{g}^R_{--}(L_R)-i=-e^{i\eta_R}\hat{g}^R_{+-}(L_R),
\end{aligned} \tag{16}$$

where η_L and η_R are arbitrary phase factors.

For the d-wave superconductor described in Fig. 1, $\Delta_L(\theta,x)=\Delta_L(x)\cos(2\theta)$ and $\Delta_R(\theta,x)=\Delta_R(x)\sin(2\theta)$. The pair interaction $V(\theta,\theta')$ in Eq. (9) has the same symmetry as the order parameter. From Eq. (9), we have

$$\Delta(x)=\frac{2T\Sigma_{n=0}^{\omega_c/2\pi T}\int_{-\pi/2}^{\pi/2}d\theta'\Sigma_{\alpha=\pm}[\lambda(\theta'_\alpha)\hat{g}_{\alpha\alpha}(x,\theta'_\alpha,\varepsilon_n)]_{12}}{\ln\left(\dfrac{T}{T_{cd}}\right)+\Sigma_{n=0}^{\omega_c/2\pi T}\dfrac{1}{n+0.5}}, \tag{17}$$

where $\Delta(x)$ means $\Delta_L(x)$ for the left-hand side (l.h.s.) ($x<0$), and $\Delta_R(x)$ for the right-hand side (r.h.s.) ($x>0$); $\lambda(\theta)=\cos(2\theta)$ for the l.h.s. and $\lambda(\theta)=\sin(2\theta)$ for the r.h.s.; ω_c is a cutoff to the summation for ε_n; The strength of the pair interaction $V(\theta,\theta')$ has been eliminated after we introduce T_{cd}—the transition temperature of the d-wave superconductor—by letting $\Delta\to0$.[29] We solve the differential Eq. (12) and the boundary conditions (14) and (16) together with Eq. (17) iteratively till the self-consistency is achieved. Before numerically solving Eq. (12), the exponentially growing part of the solution needs to be analytically

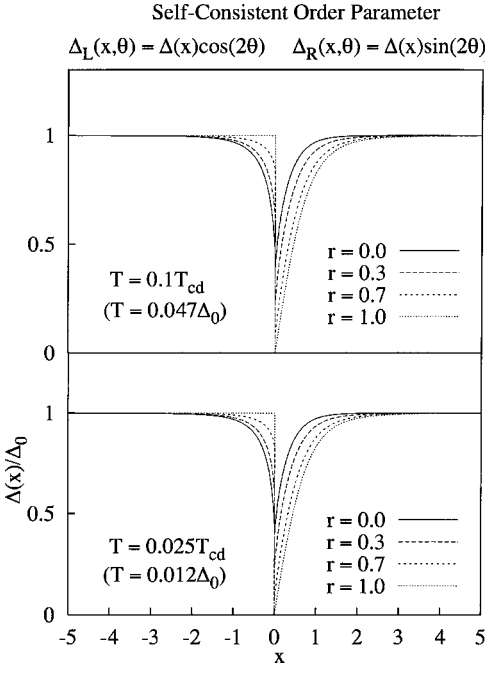

FIG. 2. Plot of the normalized self-consistent superconducting order parameter as a function of x at four values of the interface reflectivity r and two values of the temperature T. Upper panel: $T=0.1T_{cd}$; lower panel: $T=0.025T_{cd}$.

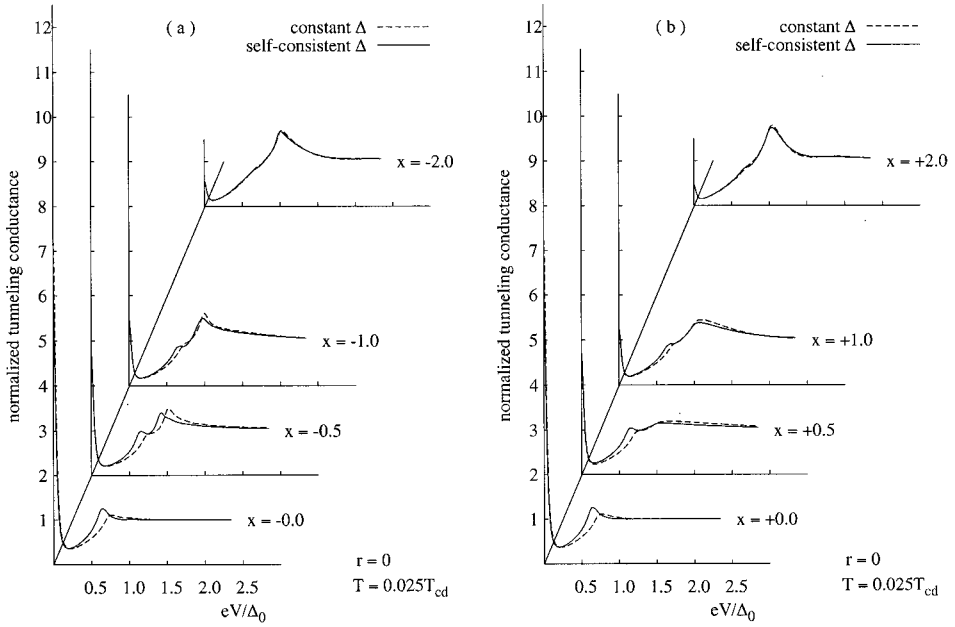

FIG. 3. Normalized local tunneling conductance G between a normal-metal STM tip and a d-wave superconductor with a $\{100\}|\{110\}$ grain boundary, as a function of the applied voltage V. Part (a) is for four values of x (in units of ξ_0) on the $\{100\}$ side (i.e., the negative x side), and part (b) is for four values of x on the $\{110\}$ side (i.e., the positive x side). The grain-boundary reflectivity parameter is assumed to be $r=0$ here, and the temperature is assumed to be $T=0.025T_{cd}$. Solid lines are obtained using the self-consistent order parameter, and the dashed lines are obtained by assuming a constant order parameter on each side. A width parameter for the quasiparticle eigenstates has been taken to be $\delta=0.05T_{cd}$. With 100% transmission at the grain boundary assumed here, the local conductance shows no discontinuity at $x=0$.

separated and removed. The technique is explained in detail in Ref. 29. On the r.h.s. of Eq. (17), the numerator and the denominator depend on the cutoff frequency ω_c. However, when ω_c is large, though both of them are divergent, their ratio is convergent. In our calculation, we have chosen $\omega_c=20\pi T_{cd}$, and we have established that the convergence has been achieved. The accuracy of the self-consistent order parameter for every point studied is four significant digits. When L_L, $L_R\rightarrow\infty$, the self-consistent order parameter is independent of the phase factors η_L and η_R, and only depends on two parameters: temperature T and the reflectivity of the interface $r\equiv|c_r|^2$.[29]

Figure 2 shows the results of the self-consistent order parameter for two temperatures, $T=0.025T_{cd}$ and $0.1T_{cd}$. For each temperature, we calculate the order parameter for four values of r: $r=0$, 0.3, 0.7, and 1. The unit of x is the coherent

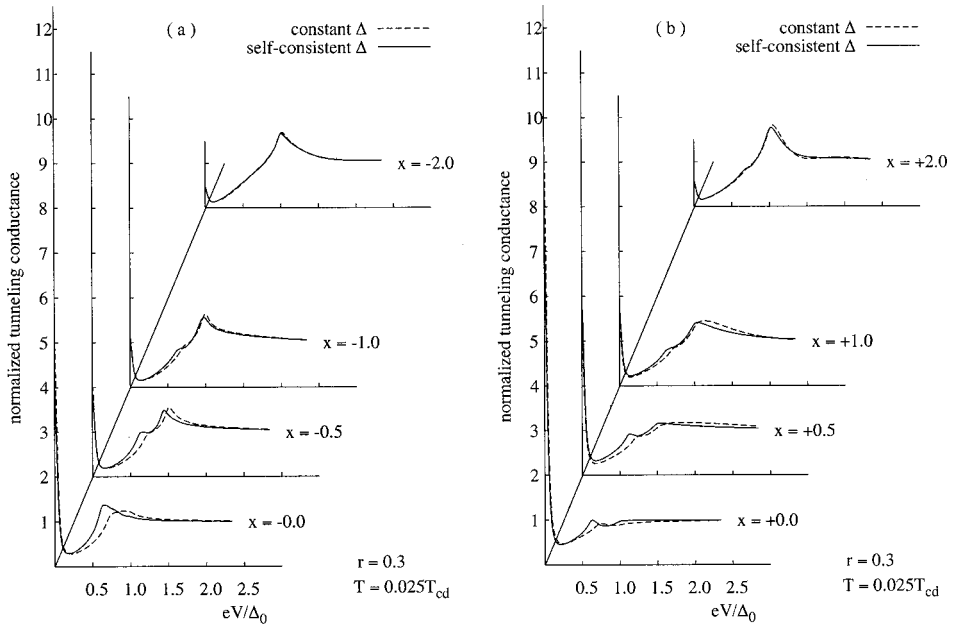

FIG. 4. Same as Fig. 3 except that $r=0.3$ in this figure. The local conductance is now discontinuous at $x=0$. That is, the plots at $x=\pm 0$ are now different.

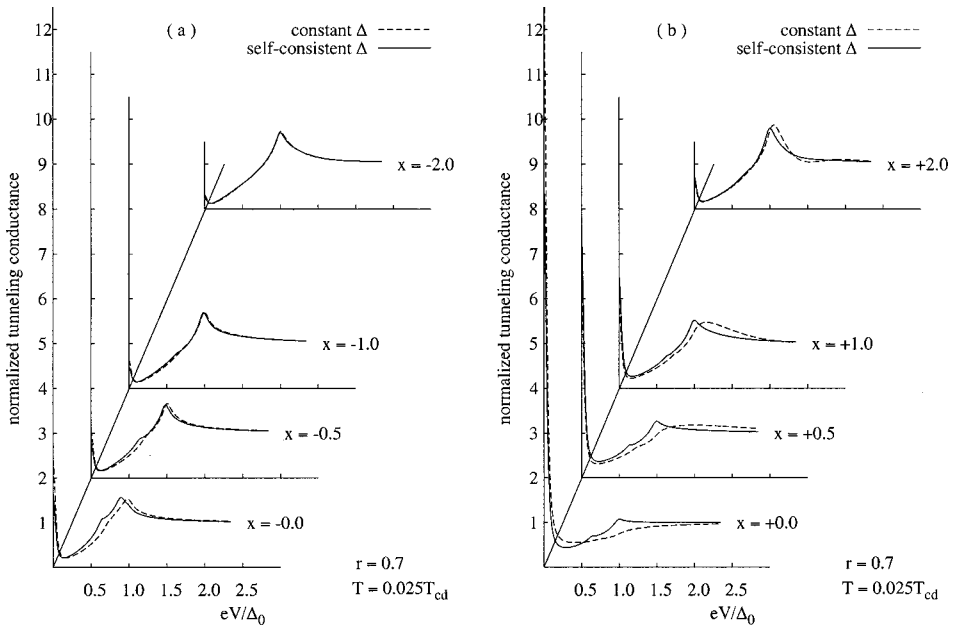

FIG. 5. Same as Fig. 4 (or 3) except that $r=0.7$ in this figure.

length $\xi_0 \equiv \hbar v_F/\Delta_0$. When $r=1$, the interface is pure reflection, so the two grains are independent of each other. In this case, the order parameter should be that of a superconductor with a specular surface on each side of the interface. The order parameter on the l.h.s. (the {100} side) is a constant, just like an *s*-wave superconductor because the incoming and outgoing quasiparticles experience the same order-parameter sign. However, for the r.h.s. (the {110} side), the reflected electrons see the sign change of the order parameter so there exists a pair breaking effect.[31] Therefore the order parameter near the interface is depressed relative to that in the bulk. In fact, it drops to zero at the interface. In the case of $r<1$, for the l.h.s., some Cooper pairs can leak into the r.h.s., which leads to some depression of the order parameter near the interface on this side. The depression increases with decreasing *r* because more Cooper pairs can leak into the r.h.s. However for the r.h.s., the depression decreases with decreasing *r* because less probability of reflection implies less pair breaking effect.

III. *N-D* TUNNELING

We extend the tunneling Hamiltonian approach used in Ref. 8 to local tunneling characteristics. The local tunneling current between a normal metal tip and the *d*-wave superconductor described in Fig. 1 can be expressed by using the

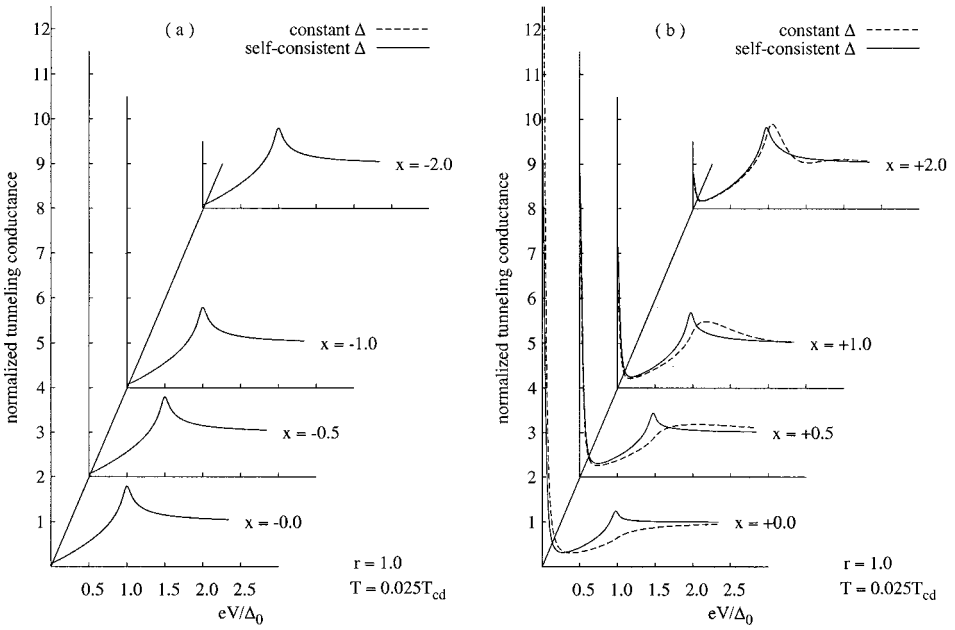

FIG. 6. Same as Fig. 4 (or 3) except that $r=1.0$ in this figure. This case corresponds to the sample split into a semi-infinite sample with a {100} surface situated at $x<0$, and a semi-infinite sample with a {110} surface situated at $x>0$. The ZBCP then shows up on the $x>0$ side only, near $x=0$, where midgap surface states exist.

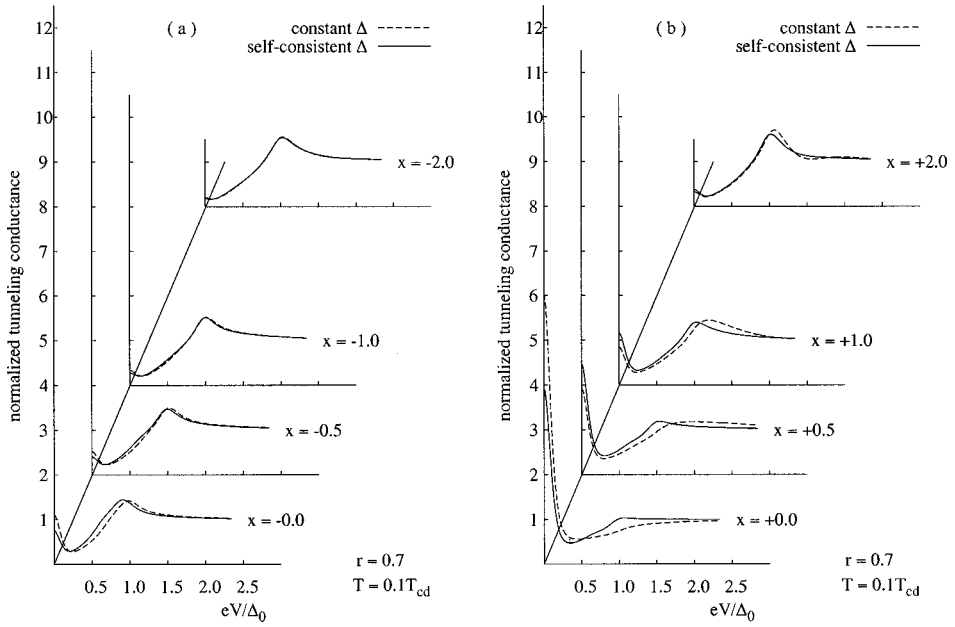

FIG. 7. Same as Fig. 5 except that the temperature $T=0.1T_{cd}$. This figure is to illustrate the temperature effect.

quasiclassical Green's function:

$$I(x,V)=\frac{1}{2\pi}\int_{-\pi/2}^{\pi/2}d\theta\int_{-\infty}^{\infty}dE\mathcal{N}(E+e\upsilon)[f(E)-f(E+eV)]$$
$$\times\mathrm{Im}[\hat{g}_{++}(x,\theta_+,E)+\hat{g}_{--}(x,\theta_-,E)]_{11}, \qquad (18)$$

where ''Im'' means the imaginary part, and ''11'' means the element 11 of the matrices $\hat{g}_{\alpha\alpha}$ $(\alpha=+,-)$. The current $I(x,V)$ has been normalized by that of the *N-N* tunneling. V is the bias voltage, and $f(x)$ is the Fermi function. $\mathcal{N}(E)$ is the normalized density of states of the counter electrode and $\mathcal{N}(E)=1$ for a normal-metal tip. $\hat{g}_{\alpha\beta}(x,\theta,E)$ is the analytical continuity of $\hat{g}_{\alpha\beta}(x,\theta,\varepsilon_n)$:

$$\hat{g}_{\alpha\beta}(x,\theta,E)=\hat{g}_{\alpha\beta}(x,\theta,\varepsilon_n)|_{\varepsilon_n\to -iE+\delta}, \qquad (19)$$

with δ being a small positive number. Inserting the Green's function $\hat{g}_{\alpha\beta}$ obtained by using the self-consistent order parameter into Eq. (18), we obtain the normalized tunneling conductance. We have calculated the tunneling conductance for eight distances (x's) from the grain boundary. Four distances are on the l.h.s. of the grain boundary (i.e., $x<0$), and the other four distances are on the r.h.s. (i.e., $x>0$). $\hat{g}_{\alpha\beta}=\hat{g}^R_{\alpha\beta}$ for $x>0$ and $\hat{g}_{\alpha\beta}=\hat{g}^L_{\alpha\beta}$ for $x<0$ in Eq. (18). The results of the normalized conductance versus the bias voltage at temperature $T=0.025T_{cd}$ and four values of r ($r=0$, 0.3, 0.7, and 1) are shown in Figs. 3–6. Part (a) gives the results for the tunneling points on the l.h.s. of the grain boundary, and part (b), the r.h.s. The corresponding results for another temperature $T=0.1T_{cd}$ and $r=0.7$ are shown in Fig. 7. We have chosen $\delta=0.05T_{cd}$ in Eq. (19) for all of the calculations.

We have also calculated the tunneling conductance by using a constant order parameter in each grain for comparison. In Figs. 3–6, the dash lines are the results obtained by using a constant order parameter for each side of the interface, and the solid lines are those by using the self-consistent order parameter. We can see that for a given r, the error in the results due to the use of the constant order parameters is larger when the tunneling point is closed to the interface. For a fixed tunneling point on the l.h.s., this error is smaller for increasing r, and when $r=1$ [Fig. 6(a)], the error reduces to exactly zero, as it should be, since for $r=1$, the l.h.s. has a free surface, and the self-consistent solution gives a constant order parameter. For the r.h.s., the error is larger for larger r due to the pair breaking property of the interface.

In these figures, $x=+0.0$ and $x=-0.0$ mean that the tunneling occurs just to the right and left side of the interface, respectively. When $r=0$, the quasiclassical Green's function is continuous across the interface, so the tunneling conductance is also continuous there. Therefore the curve for $x=-0.0$ in Fig. 3(a) is exactly the same as that for $x=+0.0$ in Fig. 3(b). When $r\neq 0$, the tunneling conductance is discontinuous across the interface because of the discontinuity of the quasiclassical Green's function there. Then tunneling characteristics at $x=+0.0$ and $x=-0.0$ are different,

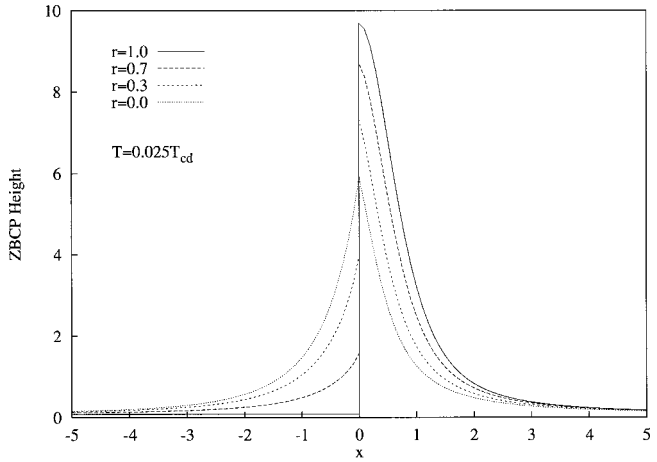

FIG. 8. The height of the ZBCP is plotted as a function of the distance x away from the interface for different values of r. $T=0.025T_{cd}$ is assumed.

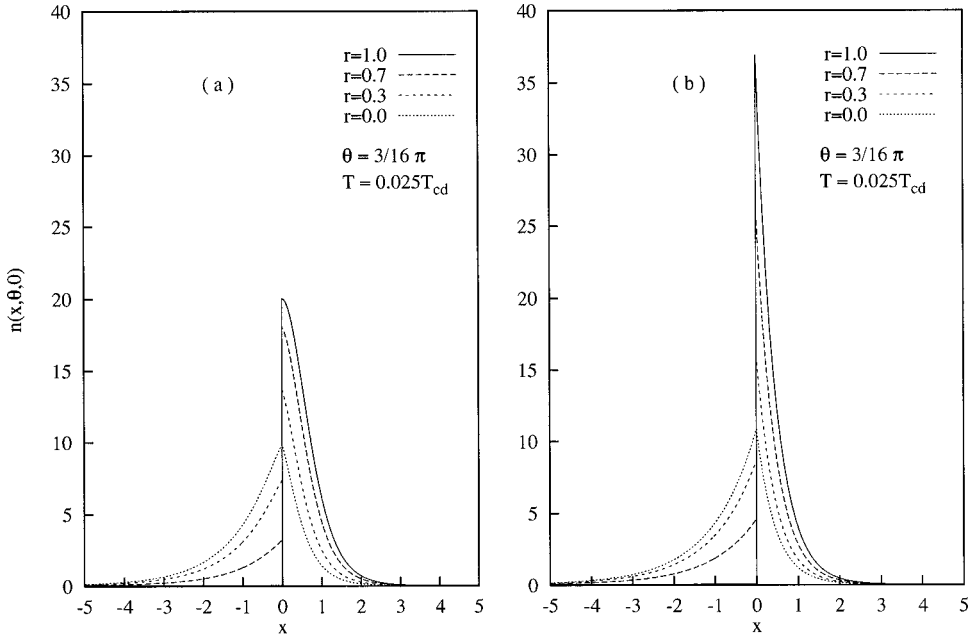

FIG. 9. Plot of $n(x,\theta,E)$ at $E=0$ as a function of x for four values of r at $\theta=(\frac{3}{16})\pi$. Part (a) is obtained using the self-consistent order parameter, and part (b) is obtained by assuming a constant order parameter in each grain.

as may be seen in Figs. 4(a) and (b), in Figs. 5(a) and (b), and in Figs. 6(a) and (b).

The ZBCP corresponds to the quasiparticles tunneling into the ZEBS's. All of these figures show that the height of the ZBCP has a maximum at the interface, and diminishes when the tunneling point moves away from the interface. Observing this behavior will clearly verify that the ZEBS's are localized around the interface. [Note that the $r=1$ case presented in Figs. 6(a) and (b) corresponds to a single-crystal sample with a free {100} and {110} surface, respectively, probed by local tunneling near the surface.] The relationship between the height of the ZBCP and the distance away from the interface for different r is shown in Fig. 8. It also shows that the l.h.s. ZBCP decreases in height, and the r.h.s. ZBCP increases in height, when r increases. The relationship between the height of the ZBCP and r reflects that between the wave function of the ZEBS's and r. We can consider the following normalized *local* density of states:[29]

$$n(x,\theta,E)=\frac{1}{4}\sum_{\alpha}\ \mathrm{Im}\{\mathrm{Tr}[\hat{g}_{\alpha\alpha}(x,\theta_{\alpha},E)\hat{\rho}_3]\}. \qquad (20)$$

For $E=0$, it gives essentially the absolute-squared wave function of the ZEBS for the given θ because practically all of the contribution to $n(x,\theta,E=0)$ is from the wave function of the ZEBS for this θ when δ in Eq. (19) is very small. (But

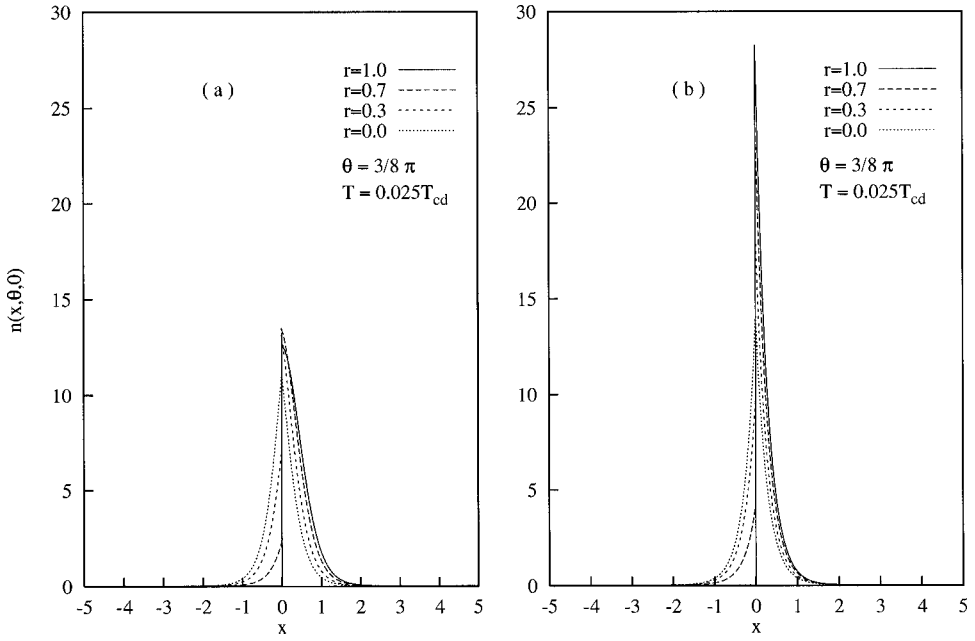

FIG. 10. Same as Fig. 9 except that $\theta=(\frac{3}{8})\pi$.

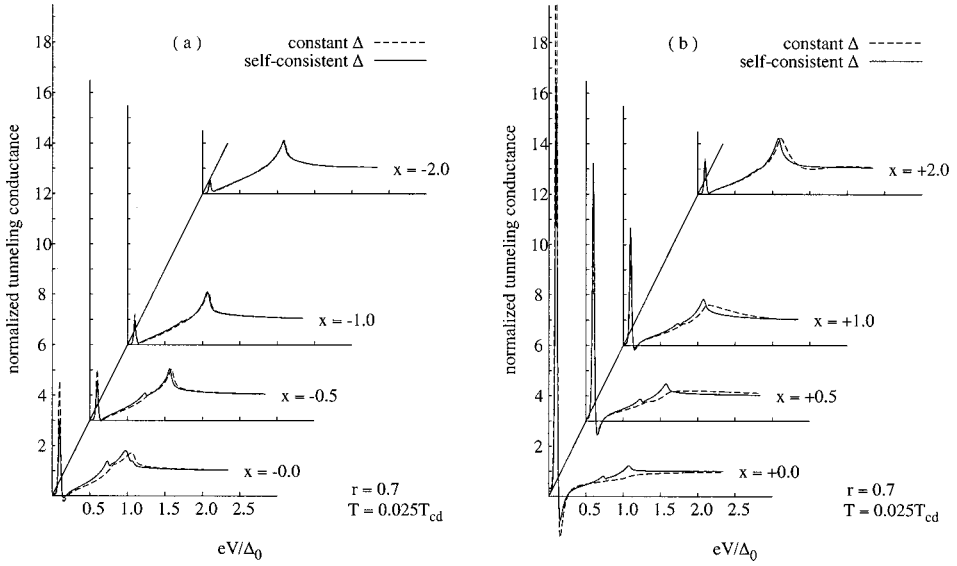

FIG. 11. Same as Fig. 5 except that the STM tip is now assumed to be made of a low-T_c s-wave superconductor with $T_{cs}=0.1T_{cd}$. The temperature $T=0.025T_{cd}$ is $\ll T_{cs}$ so we have approximated $\Delta_s(T)$ by $\Delta_s(0)$.

notice that it has its rapidly oscillating component removed already.) $n(x,\theta,E)$ in Eq. (20) has been normalized by the corresponding density of states of a normal metal. Figure 9 gives a plot of this $n(x,\theta,E=0)$ versus x for $r=0$, 0.3, 0.7, and 1, and in these figures we have chosen $\theta=(3/16)\pi$. In Fig. 9, part (a) gives the results obtained by using the self-consistent order parameter and part (b) gives those obtained by using a constant order parameter on each side of the grain boundary. It shows that $n(x<0,\theta,E=0)$ decreases, and $n(x>0,\theta,E=0)$ increases with increasing r, which corresponds to the l.h.s. ZBCP's height decreasing, and the r.h.s. ZBCP's height increasing, with increasing r, as shown in Fig. 8. [Actually, the $n(x>0,\theta,E=0)$ calculated using the self-consistent order parameter is found to decrease when r is increased, for some angles closed to π and with x near the interface, as shown in Fig. 10 for $\theta=(\frac{3}{8})\pi$. However, the ZBCP corresponds to a summation of all θ, and the contribution from this special angular range is small in comparison with that from the remaining angular range, so the relationship between the ZBCP height and r does not show this complication.] When $r=1$, only the {110} side (i.e., the r.h.s.) can have the ZEBS's. So, all of the wave functions of the ZEBS's are located on the r.h.s., which corresponds to the fact that the ZBCP is located on the r.h.s. in Figs. 6 and 8. From Fig. 9, we can also see that the quasiclassical Green's function is continuous across the interface when $r=0$ but discontinuous when $r\neq 0$.

In Ref. 9, we shall discuss the conditions for the existence of the ZEBS's for a d-wave superconductor with a grain boundary. Even though in that work we considered only a

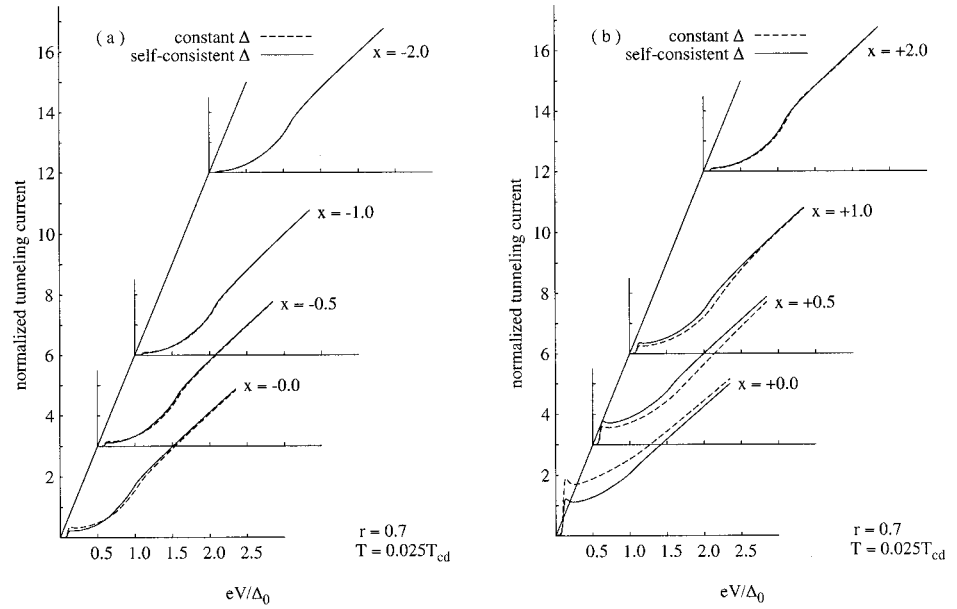

FIG. 12. The $I(V)$ characteristics corresponding to the normalized conductance plotted in Fig. 11. The current peak in this plot gives rise to the negative conductance in Fig. 11.

constant order parameter for each side of the grain boundary, the conditions obtained there are also valid for the self-consistent order parameter because of the topological nature of the ZEBS's.[4,6–8] In that work we have shown that for a *d*-wave superconductor with a {100}|{110} grain boundary, there are no ''ZEBS's'' with thir energies shifted to nonzero energies in the WKBJ approximation.[9] All of the ZEBS's will remain at zero energy when r changes to any value between 0 and 1. So the apparent subgap peak at $E\sim 1/\sqrt{2}$ in Figs. 3–7 is not due to any finite-energy bound states. In fact, it is from the interference between the effects of the order parameters on the two sides of the grain boundary: As long as $r\neq 1$, every quasiparticle can see two order parameters from the two sides of the interface. The subgap peak for constant order parameter is located at $1/\sqrt{2}$, where the quasiparticle experiences equal pair potential in both sides. The self-consistent order parameter shifts its energy away from $1/\sqrt{2}$ only slightly. When $r=1$, there is no interference between the two sides because they are completely separated. Therefore this kind of subgap peak does not appear in Fig. 6. Of course, when the orientation angles of the two sides are not as chosen here, it is possible to have some ''ZEBS's'' shifted to nonzero energies.[9] Then we expect that the ''ZBCP'' will show more complex behavior, and it will be different for different r. But it may be very difficult to observe this behavior due to the faceting problem which plagues actually grain boundaries, especially when the orientations of the grains are neither {100} nor {110}.

We have also calculated the normalized tunneling conductance at $T=0.1T_{cd}$ which is shown in Fig. 7. The behavior of the tunneling characteristics under the change of r is qualitatively the same as that at $T=0.025T_{cd}$, so we only show the results for $r=0.7$ at this temperature. Comparing with $T=0.025T_{cd}$ for each tunneling point at the same r, the height of the ZBCP is seen to be reduced and the width is somewhat broadened. When the tunneling point is two coherent lengths away from the grain boundary, the ZBCP has almost disappeared. (Notice, however, that we have defined the coherence length to be $\xi_0=\hbar v_F/\Delta_0$ here, whereas in other works it is often defined to be $\hbar v_F/\pi\Delta_0$. In that scale this point is already more than six coherence lengths away from the interface.) Because the magnitude of the order parameter at $T=0.1T_{cd}$ is almost the same as that at $T=0.025T_{cd}$, the depression and broadening of the ZBCP are practically all due to thermosmearing.

IV. *S-D* TUNNELING

In this section, we will study the case when the tip is a conventional, *s*-wave, LTSC. In this case we obtain a negative conductance for a narrow range of energy when the tunneling point is closed to the interface. Equation (18) can be directly generalized to *S-D* tunneling by using $\mathcal{N}(E)=E/\sqrt{E^2-\Delta_s^2}$ for the LTSC tip. Δ_s is the gap function (or pair potential) order parameter of the LTSC. In the following calculation, we choose $\Delta_s=0.1\Delta_0$, where Δ_0 is the maximum bulk order parameter for the *d*-wave superconductor. We calculate the tunneling current and conductance at $T=0.025T_{cd}$. Figure 11 shows the normalized tunneling conductance versus the bias voltage for $r=0.7$. There are two interesting features. The first one is that the ZBCP splits into

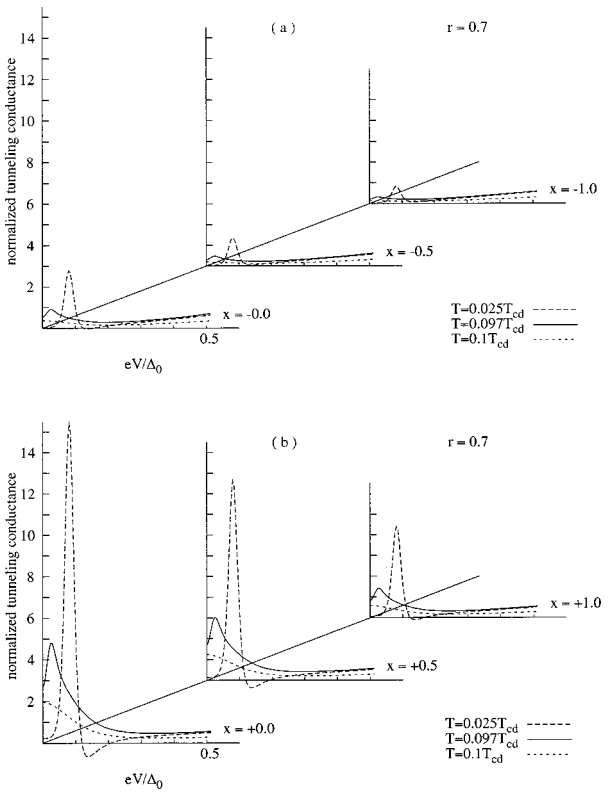

FIG. 13. Plotted is the normalized local tunneling conductance G between a low-temperature *s*-wave superconductor STM tip and a *d*-wave superconductor containing a {100}|{110} grain boundary as a function of the applied voltage V at six values of x (in units of ξ_0), showing the effect of the temperature T as it is raised from much below $T_{cs}\,(=0.1T_{cd})$ toward T_{cs}. The gap of the low-temperature, *s*-wave superconductor is seen to gradually close up in the (split) zero-bias conductance peak. Part (a) is for three values of x on the {100} side (i.e., the $x<0$ side), and part (b) is for three values of x on the {110} side (i.e., the $x>0$ side). The negative conductance just outside the split ZBCP is seen to occur only at temperatures $T\ll T_{cs}$ only.

two peaks at $eV=\pm E_s$, where E_s is essentially the gap of the *s*-wave LTSC. The second, and also the more interesting one, is that there is a range of negative conductance just outside the gap of the *s*-wave superconductor when the tunneling occurs near the interface. Figure 12 shows the corresponding *I-V* curves which exhibit current peaks. Both of the two features are due to the ZEBS's in the *d*-wave superconductor: When $eV=\pm\Delta_s$, the quasiparticles with the highest density of states in the *s*-wave superconductor side can tunnel into the ZEBS's on the *d*-wave superconductor side, so the tunneling current increases dramatically, which explains the high conductance peak at $eV=\pm\Delta_s$. When $|eV|>\Delta_s$, the quasiparticles with the highest density of states in the *s*-side tunnel into the gap region of the *d*-side, which has few available states. Only the quasiparticles with the smaller density of states in the *s*-side can now tunnel into the ZEBS's in the *d* side. Therefore the tunneling current is lower, which corresponds to the negative conductance in Fig. 11. The above discussion is similar to that on the tunneling characteristics of the conventional *S-S* tunneling,[32] but here the current peak appears at $|eV|=\Delta_s$, rather than at $|eV|=|\Delta_1-\Delta_2|$. In Fig. 11, the negative conductance has larger abso-

lute value when the tunneling point is on the r.h.s. because most part of the ZEBS wave function is localized on the r.h.s. when $r=0.7$. Hurd[33] has also obtained negative conductance for $s-d_{xy}$ tunneling. However, here we need to emphasize that because the ZEBS's are localized around a surface or interface, the negative conductance can only be observed in local tunneling near the surface or interface, and the average over even a small nonmicroscopic region of the sample can make the negative conductance disappear.[8] Sinha and Ng[20] have studied the LTSC-HTSC tunneling, and they saw the split ZBCP peaking at different energies at different temperatures. In order to qualitatively show this peak-energy shift at different temperatures, we have also calculated the tunneling conductance when the temperature is only slightly below T_{cs}, the critical temperature of the LTSC. The results are shown in Fig. 13. We see that the conductance at zero bias is dramatically increased and the splitting of the ZBCP is very small in comparison with the result at $T=0.025T_{cd}$ because the gap of LTSC is very small. (We have arbitrarily chosen the gap to be $0.1\Delta_s$, for this calculation, which corresponds to choosing $T=0.97T_{cs}$, or $T=0.097T_{cd}$, since we have let $T_{cs}=0.1T_{cd}$). Sinha and Ng[20] did not see any negative conductance. We think that it is because they studied planar junction tunneling, which measures only a spatially averaged tunneling characteristics. We predict that negative conductance can be observed if STM is used to see local tunneling characteristics, if only the tunneling point is sufficiently near a surface or an interface of a *d*-wave superconductor where ZEBS's exist.

V. CONCLUSIONS

We have studied the *local* tunneling characteristics of *N-D* and *S-D* tunneling when the *d*-wave superconductor (*D*) has a {100}|{110} grain boundary, at various positions near the grain boundary. The tunneling Hamiltonian method is used. The quasiclassical Green's-function method is used to obtain the self-consistency of the order parameter of the *d*-wave superconductor. For *N-D* tunneling, The ZBCP has the maximum height at the interface (grain boundary) and diminishes when the tunneling point moves away from the interface. The ZBCP on the l.h.s. (i.e., the {100} side) of the grain boundary decreases in height with the increase of the interface reflectivity *r*, whereas the ZBCP on the r.h.s. (i.e., the {110} side) increases in height with increasing *r*. For *S-D* tunneling, the ZBCP splits into two peaks at $E\simeq\pm\Delta_s$, which reflects the gap of the *s*-wave LTSC, and has a range of negative conductance just outside these peaks when the tunneling point is near the grain boundary. The *s*-wave gap has already been observed by nonlocalized tunneling, but we expect that this negative conductance just outside the gap feature can be observed in the STM-type of local tunneling when the tunneling point is near a surface or grain boundary of a *d*-wave superconductor where ZEBS's exist, assuming that temperature is sufficiently low, and there is not a wide damaged region near the surface or interface to suppress superconductivity there. (But superconductivity can be somewhat weakened there without losing the qualitative features predicted here.)

ACKNOWLEDGMENTS

This work was supported by the Texas Higher Education Coordinating Board (Grant No. 1997-010366-029) and by the Texas Center for Superconductivity at the University of Houston.

[1] D. A. Wollman, D. J. Van Harlingen, W. C. Lee, D. M. Ginsberg, and A. J. Leggett, Phys. Rev. Lett. **71**, 2134 (1993); C. C. Tsuei, J. R. Kirtly, C. C. Chi, L. S. Yu-Jahnes, A. Gupta, T. Shaw, J. Z. Sun, and M. B. Ketchen, *ibid.* **73**, 593 (1994); D. A. Wollman, D. J. Van Harlingen, J. Giapintzakis, and D. M. Ginsberg, *ibid.* **74**, 797 (1995); J. R. Kirtley, C. C. Tsuei, J. Z. Sun, C. C. Chi, L. S. Yu-Jahnes, A. Gupta, M. Rupp, and M. B. Ketchen, Nature (London) **373**, 225 (1995). J. R. Kirtley, C. C. Tsuei, M. Rupp, J. Z. Sun, L. S. Yu-Jahnes, A. Gupta, M. B. Ketchen, K. A. Moler, and M. Bhushan, Phys. Rev. Lett. **76**, 1336 (1996); C. C. Tsuei, J. R. Kirtley, M. Rupp, J. Z. Sun, A. Gupta, M. B. Ketchen, C. A. Wang, Z. F. Ren, J. H. Wang, and M. Bhushan, Science **271**, 329 (1996); C. C. Tsuei and J. R. Kirtley, J. Phys. Chem. Solids **59**, 2045 (1998).

[2] D. J. Van Harlington, Rev. Mod. Phys. **67**, 515 (1995).

[3] J. R. Schrieffer, Solid State Commun. **92**, 129 (1994); D. G. Scalapino, Phys. Rep. **250**, 329 (1995).

[4] C.-R. Hu, Phys. Rev. Lett. **72**, 1526 (1994).

[5] J. Yang and C.-R. Hu, Phys. Rev. B **50**, 16 766 (1994).

[6] F. Fogelstrom, D. Rainer, and J. A. Sauls, Phys. Rev. Lett. **79**, 281 (1997).

[7] Y. Tanuma, Y. Tanaka, M. Yamashiro, and S. Kashiwaya, Phys. Rev. B **57**, 7997 (1998).

[8] C.-R. Hu, Phys. Rev. B **57**, 1266 (1998).

[9] H. Zhao and C.-R. Hu (unpublished).

[10] Y. Tanaka and S. Kashiwaya, Phys. Rev. Lett. **74**, 3451 (1995).

[11] J. Geer, X. X. Xi, and G. Linker, Z. Phys. B: Condens. Matter **73**, 329 (1988).

[12] T. Walsh, Int. J. Mod. Phys. B **6**, 125 (1992).

[13] J. Lesueur, L. H. Greene, W. I. Feldmann, and A. Inam, Physica C **191**, 325 (1992).

[14] Q. Chen and K.-W. Ng, Phys. Rev. B **45**, 2569 (1992).

[15] M. Covington, R. Scheuerer, K. Bloom, and L. H. Greene, Appl. Phys. Lett. **68**, 1717 (1996).

[16] L. Alff, H. Takashima, S. Kashiwaya, N. Terada, H. Ihara, Y. Tanaka, M. Koyanagi, and K. Kajimura, Phys. Rev. B **55**, 14 757 (1997).

[17] L. Alff, H. Takashima, S. Kashiwaya, N. Terada, T. Ito, K. Oka, Y. Tanaka, and M. Koyanagi, Physica C **282-287**, 1485 (1997).

[18] J. W. Ekin, Y. Xu, S. Mao, T. Venkatesan, D. W. Face, M. Eddy, and S. A. Wolf, Phys. Rev. B **56**, 13 746 (1997).

[19] L. Alff, A. Beck, R. Gross, A. Marx, S. Kleefisch, T. Bauch, H. Sato, M. Naito, and G. Koren, Phys. Rev. B **58**, 11 197 (1998).

[20] S. Sinha and K.-W. Ng, Phys. Rev. Lett. **80**, 1296 (1998).

[21] L. Alff, S. Kleefisch, U. Schoop, M. Zittartz, T. Kemen, T. Bauch, A. Marx, and R. Gross, Eur. Phys. J. B **5**, 423 (1998).

[22] M. Covington, M. Aprili, E. Paraoanu, L. H. Greene, F. Xu, J. Zhu, and C. A. Mirkin, Phys. Rev. Lett. **79**, 277 (1997).

[23] J. Y. T. Wei, N.-C. Yeh, D. F. Garrigus, and M. Strasik, Phys. Rev. Lett. **81**, 2542 (1998).

[24] W. Wang, M. Yamazaki, K. Lee, and I. Iguchi, Phys. Rev. B **60**, 4272 (1999).

[25] S. Kashiwaya, T. Ito, K. Oka, S. Ueno, H. Takashima, M. Koyanagi, Y. Tanaka, and K. Kajimura, Phys. Rev. B **57**, 8680 (1998).

[26] It was stated in many experimental papers that the ZBCP can only be observed in *ab*-plane tunneling, and that it cannot be observed in *c*-axis tunneling. We think that such statements are misleading. Rather, we think that the only reason that the ZBCP is not observed in most *c*-axis tunneling setups is because the total spectral weight of the ZEBS's is too small to be observable in those experimental arrangements. Thus to observe the ZBCP in *c*-axis tunneling all one needs to do is to increase the spectral weight of the ZEBS's, by either increasing the surface (or interface)-to-volume ratio in the sample, or, more simply, by performing *local* tunneling using STM in the vicinity of a surface or interface. Of course the surface cannot have a thick damaged layer which is not even superconducting. But if this were the reason that the ZBCP were not observed, then the gap features should not have been observed either. The result would be the featureless, roughly V-shaped tunneling conductance curves reported in some (especially earlier) publications. Most recent *c*-axis tunneling experiments, with better prepared surfaces, were clearly not plagued by this problem, since they can all see very clear gap features.

[27] The local density of states of $N/I/D$ and $D/I/D$ junctions has been studied previously by Y. Tanaka and S. Kashiwaya [Phys. Rev. B **53**, 9371 (1996)] without taking into account the self-consistency of the order parameter.

[28] M. Ashida, S. Aoyama, J. Hara, and K. Nagai, Phys. Rev. B **40**, 8673 (1989).

[29] Y. Nagato, K. Nagai, and J. Hara, J. Low Temp. Phys. **93**, 33 (1993).

[30] Y. Ohashi, J. Phys. Soc. Jpn. **65**, 823 (1996).

[31] C. Bruder, Phys. Rev. B **41**, 4017 (1990).

[32] I. Giaever, in *Tunneling Phenomena in Solids*, edited by E. Burstein and S. Lundqvist (Plenum, New York, 1969), p. 255.

[33] M. Hurd, Phys. Rev. B **55**, R11 993 (1997).